Theoretical prediction of mechanics, transport, and thermoelectric properties of full Heusler compounds Na_2KSb and X_2CsSb (X = K, Rb)

Tongcai Yue,[1] Pengfei Sui,[1] Yinchang Zhao,[1,*] Jun Ni,[2,†] Sheng Meng,[3,‡] and Zhenhong Dai[1,§]

[1]*Department of Physics, Yantai University, Yantai 264005, People's Republic of China*

[2]*Department of Physics, Tsinghua University, Beijing 100084, People's Republic of China*

[3]*Beijing National Laboratory for Condensed Matter Physics and Institute of Physics, Chinese Academy of Sciences, Beijing 100190, People's Republic of China*

(Received 19 February 2022; revised 3 May 2022; accepted 6 May 2022; published 20 May 2022; corrected 20 January 2023)

Full Heusler compounds have become a research hotspot in the thermoelectric (TE) field, because they have the remarkable electronic properties and high-TE power factor. Nevertheless, the inherent high thermal conductivity κ_L hinders their further application as TE device. Hence, we investigate the mechanical, transport, and thermoelectric properties in Na_2KSb and X_2CsSb (X = K, Rb) with eight valence electrons per formula unit (f.u.) by using the first-principles calculations combined with self-consistent phonon (SCP) theory, compressive sensing (CS) techniques, and Boltzmann transport equation (BTE). Due to the strong three phonon scattering combined with small phonon group velocity, we obtain the ultralow lattice thermal conductivities. An evaluation of their mechanical properties reveals that they are all brittle compounds, and Rb_2CsSb has the strongest elastic anisotropy. To capture rational electron transport properties, we include the effects of the acoustic deformation potential (ADP) scattering, polar optical phonon (POP) scattering, and ionized impurity (IMP) scattering on the electron relaxation time. Finally, a high p-type ZT values of 2.74 (2.48) at 600 (900) K are captured in the cubic K_2CsSb (Na_2KSb). These findings not only help us to comprehensively understand the physical properties of full Heusler compounds with eight valence electrons per f.u., but also support them as potential candidates for thermal management and thermoelectric applications.

DOI: 10.1103/PhysRevB.105.184304

I. INTRODUCTION

At present, energy shortage, environmental pollution, and the social problems caused by them have become the biggest challenges facing mankind and science [1,2]. Taking into account the nonrenewable fossil resources and the increasing attention in environmental issues, scientists have conducted in-depth research on alternative methods of efficient, sustainable, and environment-friendly power generation. The research of thermoelectric (TE) materials has become a current hot topic, because TE technology has the advantage of directly converting heat sources into electrical energy without causing additional pollution [3–6]. The TE conversion efficiency of materials can be evaluated by the figure of merit

$$ZT = \frac{S^2\sigma T}{\kappa_L + \kappa_e}. \quad (1)$$

Among them, the S, σ, T, and κ_L (κ_e) denote the thermopower, electrical conductivity, temperature, and lattice (electrical) thermal conductivity, respectively. Consequently, we can improve ZT value through adjusting the contradictory material properties by simultaneously boosting the power factor (σS^2) and lowering the total (lattice plus electrical) thermal conductivity. The former is usually realized through carrier energy filtering approach [7,8] and band alignment [9,10], while the latter prefers sublattice disordering [11], ferroelectriclike lattice instability [12,13], nanostructuring [14], anharmonicity [15,16], and structural complexity [17,18].

In the last ten years, full Heusler (FH) compounds with semiconducting behavior have been extensively studied in the TE field, because of their attractive electronic properties with high PF. Traditional FH semiconductors contain 24 valence electrons per molecular formula unit (f.u.), which is composed of main III to V groups and transition metal elements. Generally, these FH semiconductors have high TE power factor, especially, Fe_2VAl even exceeds 10 mW m^{-1} K^{-1} by using band engineering [19]. However, their intrinsic high lattice thermal conductivities κ_L have hindered the research and application of TE materials since they were discovered [20–22]. Recently, a series of new FH semiconductors with ultralow κ_L have been discovered [23]. These compounds contain 10 valence electrons per f.u., and are composed of alkaline earth metals, noble metals, and IV or V main group elements. Due to the coexistence of extremely low κ_L and high PF, these FH compounds capture high ZT, e.g., n-type Sr_2AuSb with a ZT ∼4.4 at 750 K [24], n-type Ba_2AuBi with a ZT ∼5 at 800 K [25], n-type Sr_2AuAs with a ZT ∼3.3 at 700 K [26], etc. However, the above FH compounds contain the rare noble metals (Au), which greatly increase the cost of TE materials. Additionally, another class of FH semiconductor that

*Second corresponding author: y.zhao@ytu.edu.cn
†junni@mail.tsinghua.edu.cn
‡smeng@iphy.ac.cn
§First corresponding author: zhdai@ytu.edu.cn

has 8 valence electrons per f.u. is always neglected, e.g., Na_2KSb [27], K_2CsSb and Rb_2CsSb [23,28]. Compared to the FH semiconductors with 24 valence electrons per f.u., these FH semiconductors with eight valence electrons per f.u. have ultralow κ_L and higher ZT. Meanwhile, they do not contain rare noble metal elements (Au) and toxic elements (Hg), which are more conducive to large-scale applications. Furthermore, K_2CsSb and Rb_2CsSb can be successfully prepared by deposition sputtering [29–32]. Hence, these are more suitable as TE materials than semiconductors with 10 and 24 valence electrons per f.u..

Here, we employ the first-principles calculations to comprehensively investigate the mechanical, transport, and thermoelectric properties of the FH compounds Na_2KSb, and X_2CsSb (X = K, Rb). Theoretical calculations indicate that these three FH compounds are mechanical stable, and Rb_2CsSb has strong elastic anisotropy. Since the harmonic (HA) approximation is failure to treat serious anharmonic materials, e.g., K_2CsSb and Rb_2CsSb, we employ self-consistent phonon (SCP) theory to calculate the thermal transport properties by considering the temperature-dependent renormalization of phonon energies. The calculated results suggest that these three FH compounds have ultralow κ_L due to the rattling modes of alkali-metal atoms [33,34]. Meantime, the alkali-metal atoms with strong quartic anharmonicity play an important role in the dynamical stability in K_2CsSb and Rb_2CsSb, and lead to the obvious hardening of low-lying acoustic phonon branches in Na_2KSb. With the increase of the atomic number of alkali metals, the lattice (cubic and quartic) anharmonicity increases. On the other hand, the electropositive alkali-metal atoms offer electrons to the Sb atomic framework, and Sb atomic framework connected by covalent bonds maintains the high electrical conductivity σ and carrier mobility μ of these three FH compounds [35,36]. As a result, we captured an anomalously high electrical mobility μ_e in n-type cubic Na_2KSb by including the effect of acoustic deformation potential (ADP) scattering, polar optical phonon (POP) scattering, and ionized impurity (IMP) scattering. Additionally, we obtained a high p-type ZT of 2.74 (2.48) at 600 (900) K in the FH compounds K_2CsSb (Na_2KSb). This paper emphasizes the importance of the chemical control of bonding to capture the ultralow κ and good TE performance, and clarifies the microscopic origin of the ultralow κ in these FH compounds.

II. METHODOLOGY

The FH compounds Na_2KSb, K_2CsSb, and Rb_2CsSb crystallize into the cubic Cu_2MnAl-type structure with the space group $Fm\bar{3}m$, as shown in Fig. 1(a). Among them, the X (X = Na, K, and Rb), Y (Y = K and Cs), and Sb atoms take up the Wyckoff positions $8c(\frac{1}{4}, \frac{1}{4}, \frac{1}{4})$, $4b(\frac{1}{2}, \frac{1}{2}, \frac{1}{2})$, and $4a(0, 0, 0)$, respectively. The theoretical and experimental lattice constants for these three FH compounds are listed in Table I. For the involved first-principles calculations, the projector augmented wave (PAW) potentials [37] were performed to describe the interaction of the valence electrons and ionic cores on the basis of the density functional theory (DFT). The exchange-correction energy of DFT was treated based on the generalized gradient approximations of PBEsol [38],

TABLE I. Calculated lattice parameters (a^{opt}), dielectric permittivity tensors (ϵ^{∞}), Born effective charges (Z^*), and band gaps E_g^{HSE06} for FH compounds Na_2KSb, K_2CsSb, and Rb_2CsSb. The experimental lattice parameters (a^{expt}) were also listed for comparison.

X_2YSb	Na_2KSb	K_2CsSb	Rb_2CsSb
a^{opt} (Å)	7.69	8.55	8.81
a^{expt} (Å)	7.72 [43]	8.61 [44,45]	
ϵ^{∞}	8.55	7.46	7.73
$Z^*(X)$	1.04	0.93	0.89
$Z^*(Y)$	0.99	1.23	1.35
$Z^*(Sb)$	−3.07	−3.10	−3.12
E_g^{HSE06}	1.38	1.70	1.13

implemented in the VASP package [39,40]. The cutoff energy of the plane-wave basis set is set to 500 eV in the all calculations. Initially, the optimum structures of these three FH compounds are captured in a Γ-centering 13 × 13 × 13 **k**-point mesh. In order to obtain the accurate atomic force, the energy convergence standard of electronic self-consistent-loop was 10^{-8} eV, and the convergence criterion of the whole force is less than 10^{-4} eV/Å. The thermal stability of these three FH compounds were tested by performed *ab initio* molecular dynamics (AIMD) simulations in a 2 × 2 × 2 supercell with 2 × 2 × 2 k-point mesh, as shown in Fig. S1 in the Supplemental Material [41]. The time was set to 5000-step and interval was 2 fs. Density functional perturbation theory (DFPT) is used to calculate nonanalytical corrections caused by dipole-dipole interactions, which usually results in longitudinal-transverse optical (LO-TO) splitting in polar semiconductors [42]. The calculated Born effective charge and dielectric permittivity tensor are listed in the Table I. Furthermore, the HA interatomic force constants (IFCs) were captured by virtue of the finite displacement approach [46]. The anharmonic IFCs were trained based on the CS techniques [47]. For details, please refer to the Supplemental Material [41]. Subsequently, the temperature-dependent anharmonic phonon energies were captured by using SCP calculations combined with obtained second-order to sixth-order IFCs. Finally, within a 14 × 14 × 14 **q**-point mesh, the lattice thermal conductivity of these three FH compounds were estimated using Boltzmann transport equations (BTE) of relaxation time approximation (RTA). The above IFCs and lattice thermal conductivity calculations were implemented in ALAMODE code [48,49]. The κ_L was written as

$$\kappa_L = \kappa_L^{\alpha\beta}(\mathrm{T}) = \frac{1}{N\Omega}\sum_{q,j} C_{q,j}(T)\upsilon_{q,j}^{\alpha}\upsilon_{q,j}^{\beta}\tau_{q,j}(\mathrm{T}), \qquad (2)$$

where Ω, N, $\alpha(\beta)$, q, j, $C_{q,j}$, $\upsilon_{q,j}^{\alpha(\beta)}$, and $\tau_{q,j}(\mathrm{T})$ denote unit cell volume, particle number, Cartesian coordinates, phonon modes, specific heat capacity, phonon group velocity, and phonon lifetime, respectively.

The AMSET code [50] was employed to calculate the mode-dependent electron-phonon scattering matrix elements g_{nm} (**k**, **q**) and electron transport properties. The initial DFT calculations for Fourier interpolation were performed within a Γ-center **k**-point mesh of 12 × 12 × 12. We use the PBE

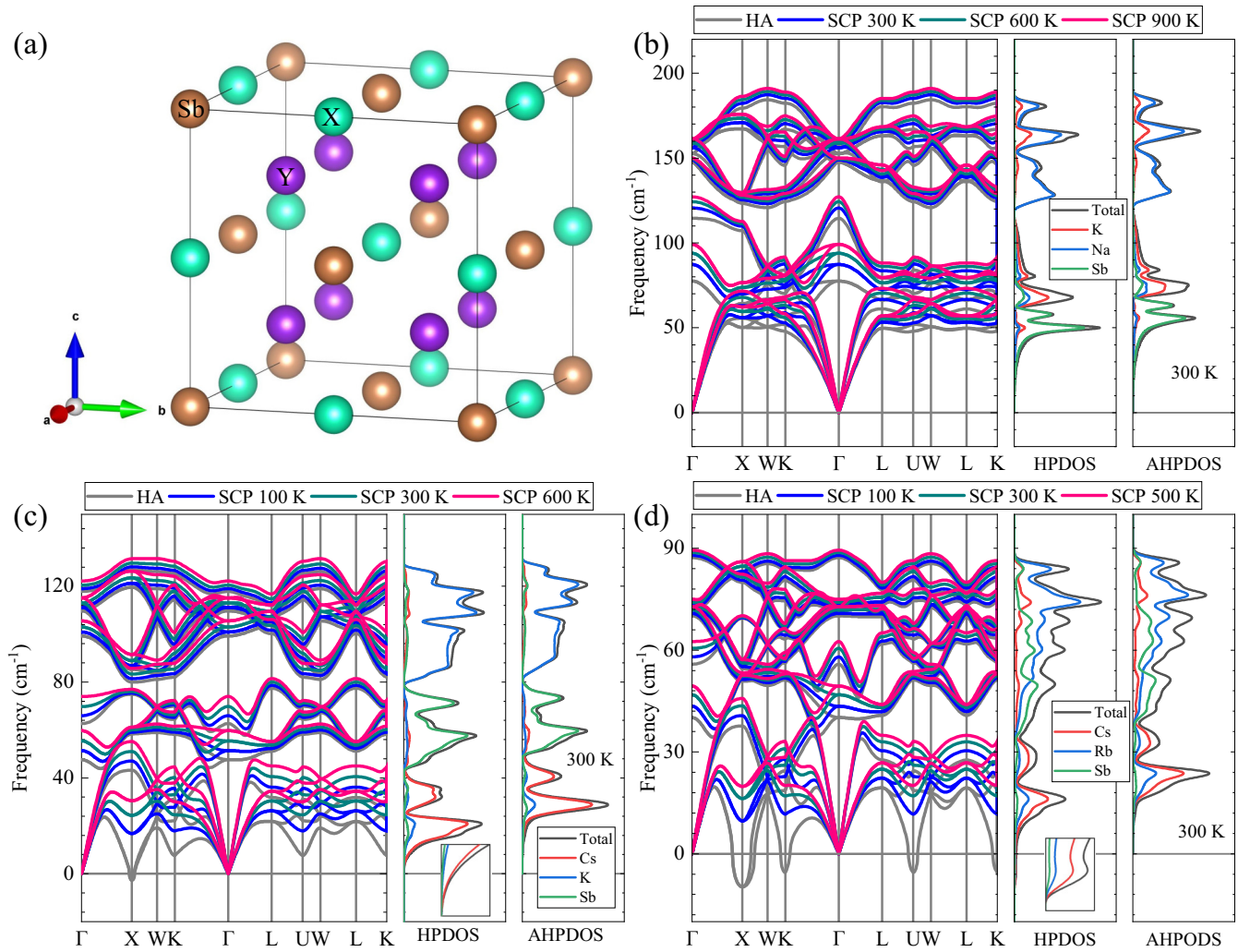

FIG. 1. (a) Crystal structure of X_2YSb (X = Na, K, Rb; Y= K, Cs) was visualized using VESTA [59]. The calculated phonon dispersions and corresponding phonon density of states (PDOS) at different temperatures for (b) Na_2KSb, (c) K_2CsSb, and (d) Rb_2CsSb, where the result of HA represents the 0 K.

functional to calculate electronic band structure, high frequency dielectric constants, and deformation potentials. We use DFPT calculations to capture elastic constants, static dielectric constants, and effective polar phonon frequency. Afterwards, to capture an accurate electron band gap, the HSE06 calculations were used. Importantly, the precise g_{nm} (**k**, **q**) was solved using a dense interpolated 101 × 101 × 101 **k**-point mesh combined with the material parameters of first-principles calculations [51]. The electron relaxation time comes from the effect of fully anisotropic acoustic deformation potential (electron-acoustic phonon interaction), polar electron-phonon (electron-ploar optical phonon interaction), and ionized impurity scattering. Finally, the calculated energy eigenvalues, group velocities, and scattering rates were used to capture rational electron transport properties using linearized BTE. Since the Lorenz constant varies with dopant concentration, we use the linear BTE to calculate the κ_e, as shown in Eqs. (S9) in the Supplemental Material [41]. More details and material parameters can be found in Fig. S2, Fig. S3, and Table S1 in the Supplemental Material [41].

III. RESULTS AND DISCUSSION

The harmonic phonon (HP) dispersions of three FH compounds are plotted by gray lines in Fig. 1. With increasing the alkali-metal atomic number, the low-frequency acoustic modes are mainly dominated by the vibration of alkali-metal atoms, and the energies of the low-lying phonon modes associated with alkali-metal atoms decrease. When the heaviest Cs occupy the center of unit cell, K_2CsSb and Rb_2CsSb become unstable, that is, $\omega_q^2 < 0$. Analogous to the Ba_2AuBi and clathrates [23,52], the low-lying modes can be described as rattling motions of Cs (K) atoms inside the pseudocage structure comprised of the alkali-metal atoms X_2 (X = Na, K, Rb) and Sb atoms. Because of the dynamic coupling of the rattling atoms to the rigid lattice framework, the acoustic and optical branches separated by a small gap [53,54]. The phenomenon is so called "avoided crossing", which can be clearly observed in Fig. S9 in the Supplemental Material [41]. Furthermore, the electron localization function (ELF) indicate that localized Y-site atoms causes weak interaction with Sb

TABLE II. The calculated elastic constants C_{ij} (GPa), bulk modulus B (GPa), shear modulus G_{VRH} (GPa), Young's modulus E (GPa), and Debey temperature θ_D (K) for the cubic Na_2KSb, K_2CsSb, Rb_2CsSb. Other theoretical works are also listed for comparison.

Semiconductor	C_{11}	C_{12}	C_{44}	B	G_V	G_R	G_H	E	θ_D
Na_2KSb	32.94	14.18	17.90	20.44	14.49	13.13	13.81	33.81	231.0
Other (Na_2KSb[a])	32.18	12.82	20.27						
Other (Na_2KSb[b])	22.28	19.3	17.59	20.35	1.26(11.13)	3.21	7.17(7.17)	19.25	
K_2CsSb	22.40	10.06	12.13	14.18	9.74	8.75	9.25	22.78	157.2
Other (K_2CsSb)	38.24	3.13	23.29	14.68	0.73(21)	20.61	20.79(20.8)	42.52	
Rb_2CsSb	17.65	10.23	11.73	12.70	8.52	6.29	7.40	18.60	126.6
Other (Rb_2CsSb)	18.00	10.87	13.01	13.25	0.34(9.23)	6.31	7.77(7.77)	19.51	

[a]Reference [57].
[b]Reference [58].

atoms, while there is a strong interaction between Sb atoms, see Figs. S4(a) and 4(b) in the Supplemental Material [41]), making Cs (K) atoms behave as an inert alkaline-earth metals in tetrakaidecahedral cages.

The finite-temperature phonon dispersions for three FH compounds have been calculated using SCP theory under various temperatures, and the results are illustrated in Figs. 1(b)–1(d). Generally, the quartic anharmonicity increases the energies of low-lying phonon modes, which can be attributed to the dominant and positive contribution from the diagonal term of quartic coefficient. With increasing alkali-metal atomic number, the quartic anharmonic effect is more important for the phonon energies, exhibiting a more pronounced hardening of the phonon frequencies. Like the guest atoms of clathrates [52], the alkali-metal atoms at the Y position have an anomalously strong quartic anharmonicity, which play a vital role in the dynamical stability of K_2CsSb and Rb_2CsSb, and PDOS at 300 K also confirms this point. In addition, the thermal stability of these three FH compounds are also discussed, and the results indicate that Na_2KSb, K_2CsSb and Rb_2CsSb are stable at 900 K, 600 K, and 500 K, respectively. Moreover, the calculated elastic constants for these three FH compounds satisfy the mechanical stability criteria of cubic lattice system

$$C_{11} - C_{12} > 0; \qquad C_{11} + 2C_{12} > 0; \qquad C_{44} > 0, \tag{3}$$

revealing that they are mechanically stable [55,56]. The calculated elastic constants using the strain-stress approach are shown in Table II. Our results are in good agreement with other studies [57,58] except the elastic constants of K_2CsSb. The difference requires experimental investigation on elastic properties of K_2CsSb.

Analogously to the skutterudites and clathrates, the guest atoms with rattling vibration will hinder heat conduction in the host cages, resulting in low κ_L. Hence, the κ_L of these three FH compounds are calculated by including the quartic anharmonic renormalization of phonon energies, three-phonon scattering, isotope scattering, and 1-mm grain boundary scattering, as shown in Fig. 2. For Na_2KSb, the κ_L of the HP+BTE is also displayed in Fig. 2. The κ_L using SCP+BTE is obviously higher than the result of HP+BTE, which can be attributed to the increase in phonon group velocity and the suppression of the three-phonon scattering phase spaces caused by phonon frequencies renormalization [60]. If the four-phonon scattering caused by the quartic anharmonicity is considered, the κ_L decreases [60,61]. Meanwhile, the TE properties of materials will be further improved. Since K_2CsSb and Rb_2CsSb have imaginary frequencies at zero temperature, the HA many-body perturbation theory is invalid. These three FH compounds exhibit ultralow κ_L (0.31–0.95 W $m^{-1} K^{-1}$ at room temperature) using SCP+BTE, which are lower than previous theoretical [23,62] and experimental [63,64] values of FH compounds. This finding is exciting, because such a low κ_L can only be found in complex structures [65,66]. More importantly, the κ_L of these three FH compounds exhibit lower temperature dependence after considering the quartic anharmonic renormalization of phonon frequencies, especially for K_2CsSb. The temperature dependence of κ_L can be approximately described by $\kappa_L \propto T^{\eta}$. Among them, the η values of SCP+BTE are 0.78 for Na_2KSb, 0.55 for K_2CsSb, and 0.63 for Rb_2CsSb, respectively. Generally, the κ_L of most materials is proportional to T^{-1} [67]. While the results of HP+BTE have high η, the η value of Na_2KSb is 1.03. The consideration of quartic anharmonic renormalization of phonon frequencies gives rise to a weaker temperature dependence. This underestimated temperature dependence suggests that it is necessary to account for four-phonon scattering. If four-phonon scattering is

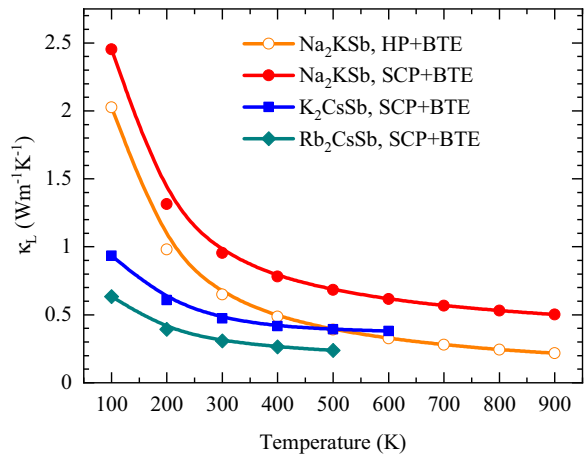

FIG. 2. Temperature-dependent κ_L of the three FH compounds calculated using SCP+BTE. For Na_2KSb, the result of HP+BTE is also shown for comparison. The 1-mm grain boundary scattering is also considered.

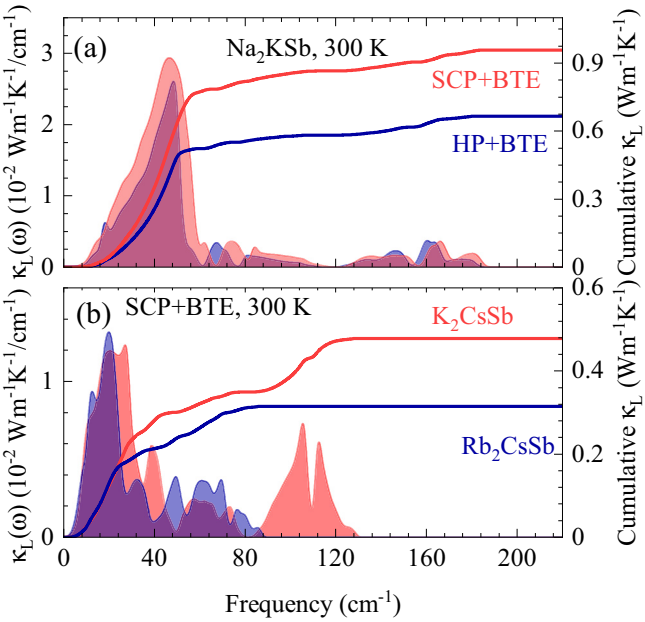

FIG. 3. Lattice thermal conductivity spectrum κ_L (ω) and relevant cumulative κ_L for the three FH compounds Na_2KSb, K_2CsSb, and Rb_2CsSb.

considered, the temperature dependence will become stronger, e.g., approaching T^{-1}. Additionally, the TE properties of the material will be further enhanced due to the reduced κ_L.

Subsequently, we explored the key components entering phonon BTE, namely, phonon frequencies (ω_{ph}), phonon group velocity (υ_{ph}), and phonon lifetime (τ_{ph}) to investigate the microscopic origin of low κ_L. Initially, We compared the lattice thermal conductivity spectrum [κ_L (ω)] and corresponding cumulative κ_L for these three FH compounds at 300 K, and the calculated results are shown in Fig. 3. As the alkali-metal atomic number increases, the highest phonon frequencies and Debey temperature (see Table I) decrease significantly. The Debye temperature ($\theta_D = \frac{\hbar\omega_D}{k_B}$) can usually describe the vibration of crystal lattice, where $\hbar$ is reduce Planck's constant, ω_D is Debey frequency, and k_B is Boltzmann constants, respectively. After careful investigation, we find that these decreases can be attributed to the increase in atomic mass and decrease in interatomic strength [68–70], which leads to small atomic displacements. Meantime, the reduction of the highest phonon frequencies makes the optical phonon branches more inclined to suppress the acoustic phonon branches, thus hindering the propagation of heat-carrying phonons. Concretely, because of the "avoided crossing" phenomenon, the reduction of the highest phonon frequencies makes the optical phonon branches more inclined to suppress the acoustic phonon branches, e.g., the acoustic phonon branches becomes flatter. The flatter acoustic phonon branches not only reduce the phonon group velocity, but also lead to enhancement of energy-conserving and momentum-conserving phase spaces. Compared the two results of Na_2KSb (HA and SCP) with the frequencies increasing of the low-lying modes caused by alkali-metal atoms, κ_L (ω) evidently increases below 80 cm^{-1}, and the peak values of κ_L (ω) increase evidently. Furthermore, quartic anharmonicity mainly affects the low-frequency acoustic phonon mode, but has little effect on the high-frequency optical phonon mode. At the same time, the results of cumulative κ_L show that the low-frequency phonon mode provides the main contribution to the κ_L of the three FH compounds.

To further illustrate the variation of κ_L (ω), we calculated thermal transport parameters of the three FH compounds, including phonon group velocity (υ_{ph}), phonon lifetime (τ_{ph}), Grüneisen parameter (γ), and three-phonon scattering phase space (W), and the calculated results are shown in Figs. S2 and S3 in the Supplemental Material [41]. The results indicate that the low κ_L is the result of low υ_{ph} combined with small τ_{ph}. Generally, the υ_{ph} is more important because $\kappa_L \propto \upsilon_{ph}^2$. As the alkali-metal atomic number increases, phonon frequencies ω_{ph} softens, the υ_{ph} decreases evidently, because υ_{ph} can be written as $\upsilon_{ph} = \frac{d\omega}{dq}$. Furthermore, considering the quartic anharmonic renormalization of phonon energies, the υ_{ph} under low frequencies phonon modes increases significantly, which is consist with the hardening of low-lying modes under low frequencies. Analogously to *Cmcm* phase SnSe, small υ_{ph} means low κ_L in these three FH compounds. Next, the effect of τ_{ph} is discussed, because the κ_L is proportional to the τ_{ph} of materials, we can study the influence of phonon lifetime on the thermal conductivity of materials. Based on the Matthiessen's rule, the total τ_{ph} can be written as is

$$\tau_{ph}^{-1}(T) = 2\left(\Gamma_{ph}^{anh}(T) + \Gamma_{ph}^{iso} + \frac{|\upsilon_{ph}|}{L}\right), \quad (4)$$

where $\Gamma_{ph}^{anh}(T)$ is cubic anharmonic phonon linewidth, Γ_{ph}^{iso} is isotope effect phonon linewidth, and L is grain boundary size with the values of 1 mm, respectively. Since the 1-mm grain boundary slightly increases the total scattering rate, we consider the calculated results to be an upper limit for the κ_L and a lower limit for the ZT value. Additionally, to better illustrate the effect of grain boundary scattering on κ_L, we provide the κ_L and grain boundary scattering rate as functions of grain size, as shown in Fig. S10 in the Supplemental Material [41]. It can be seen that as grain boundary size decreases, grain boundary scattering increases, resulting in a significant decrease in κ_L. The decrease in κ_L is more severe at low temperature, which can be attributed to the weakened three-phonon scattering at low temperature. As the alkali-metal atomic number increases, the τ_{ph} decreases, which can be put down to the increase in the γ and W. The former is usually used to describe cubic anharmonicity of solids, which can be directly measured through experiments. The latter represents the number of three-phonon scattering processes. Taking quartic anharmonic renormalization of phonon frequencies into account, the τ_{ph} increases, which is mainly due to reduced γ. As a result, the coexistence of small υ_{ph} and τ_{ph} results in extremely low κ_L. As the atomic number increases, not only the quartic anharmonicity increases significantly, but the cubic anharmonicity also increases significantly.

Since the FH compounds can be easily alloyed and nanostructured, the κ_L of the three FH compounds will further decrease using structural engineering. We also calculated the cumulative κ_L, which is a function of the maximum phonon mean free paths (MFP), as shown in Fig. S5 in the Supplemental Material [41]. To investigate the experimental feasibility of

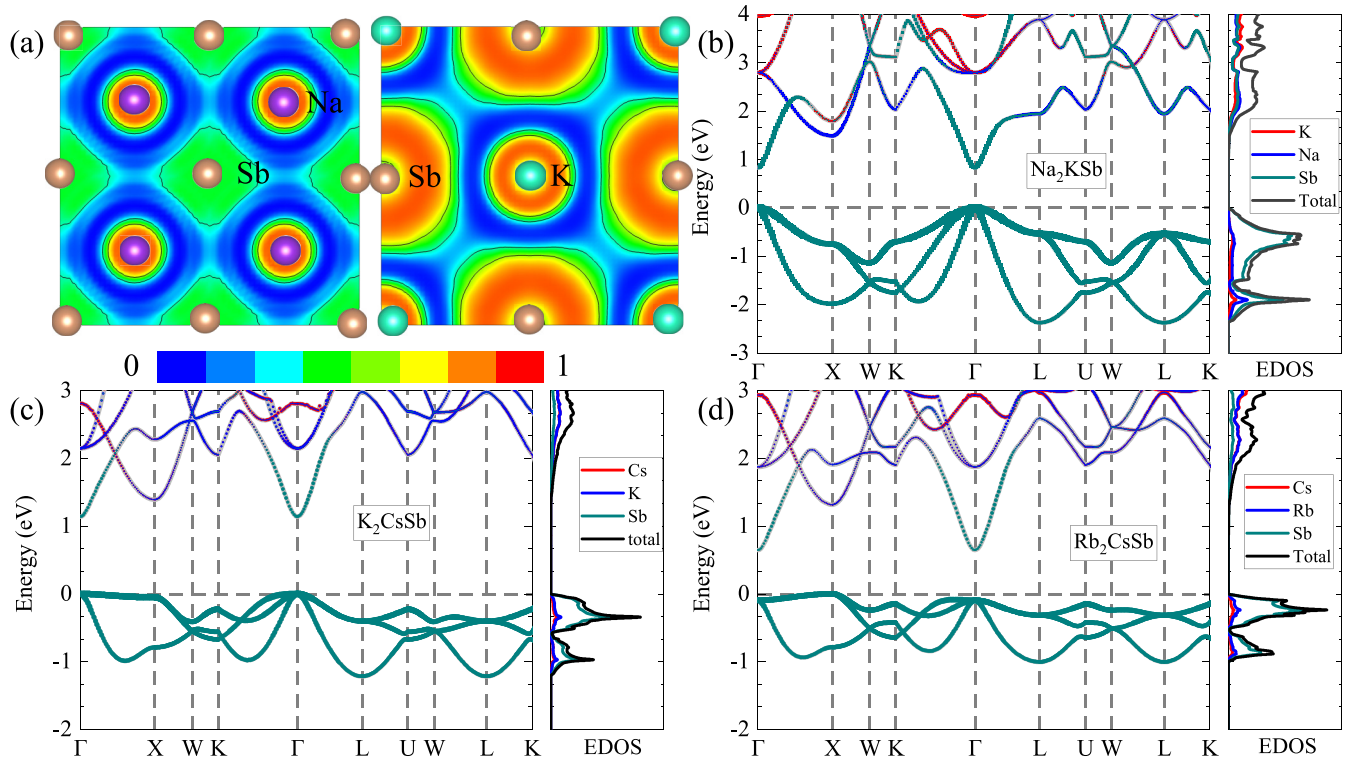

FIG. 4. (a) The projected electron localization function (ELF) in (001) plane for Na_2KSb visualized using VESTA [59]. The distances from the origin are $\frac{a}{4}$ (left) and $\frac{a}{2}$ (right), respectively. The values of the ELF range from 0.0 to 1.0, in which 1.0 signify that electrons localized completely. The electron band structure and relevant electron density of states for (b) Na_2KSb, (c) K_2CsSb, (d) Rb_2CsSb.

nanostructuring to reduce κ_L, Based on logistic curve [71], we calculated the phonon effective MFP of the three materials. The logistic curve is written as

$$\kappa_L(\Lambda \leqslant \Lambda_{\max}) = \frac{\kappa_L}{1 + \frac{\Lambda_0}{\Lambda_{\max}}}, \tag{5}$$

where $\kappa_L(\Lambda \leqslant \Lambda_{\max})$, Λ_0, and $\Lambda_{\max}$ are cumulative κ_L, phonon effective MFP, and maximum MFP, respectively. The effective MFP at 300 K is 14.1, 6.8, 5.1 nm for Na_2KSb, K_2CsSb, Rb_2CsSb, respectively. Generally, scattering through nanostructuring takes precedence over three-phonon scattering at length scales comparable to phonon effective MFP. The calculations show that Na_2KSb can effectively reduce κ_L through nanostructuring, while the other two materials are not so effective. Furthermore, if the electron MFP is comparable to the phonon effective MFP, nanostructuring also reduces σ, thereby compromising TE performance. Recently, Hosseini and coworkers found that this detrimental effect can be addressed by fine tuning the carrier concentration and judiciously designing the pore size and shape [72,73]. The electronic filtering created by such nanoscale porosity can increase the S, thereby offsetting the decrease in σ. Furthermore, the mechanical properties for these three FH compounds are investigated using the Voigt-Reuss-Hill (VRH) method [74–76], and the results are listed in Table II. As the atomic number of alkali-metal increases, the mechanical parameters of these three FH compounds decrease, including bulk modulus (B), shear modulus (G), and Young's modulus (E). The above results can be explained by the decrease in interatomic bonding strength, as shown in Fig. 4, Figs. S4(a) and S4(b) in the Supplemental Material [41]. Moreover, the ductility and brittleness of these three FH compounds are evaluated by Pugh's ratio (B_H/G_H) [77] and Poisson's ratio (ν) [78], as shown in Table III. If the former (the latter) is greater than 1.75 (0.26), the compound is a brittle material, otherwise, the compound is a ductile material. It can be seen from dual results of these three FH compounds that they are all brittle materials. Generally, significant mechanical anisotropy may cause microcracks in the material [79]. Therefore, mechanical anisotropy is an important physical quantity to improve the durability of materials. In our paper, the universal anisotropic index A^U and percent anisotropic of shear modulus A_G are used, as shown in Table III. The deviation of the above physical value from zero is used to judge the anisotropy of the material. The calculated results indicated that Rb_2CsSb has strong shear modulus anisotropy. The strong shear modulus anisotropy causes Rb_2CsSb to have larger mechanical anisotropic properties. In addition, other

TABLE III. The calculated Pugh's ratio B_H/G_H, Poisson's ratio ν, universal anisotropic index A^U, and percent anisotropic of shear modulus A_G for three cubic FH compounds Na_2KSb, K_2CsSb, and Rb_2CsSb.

Semiconductor	B_H/G_H	ν	A^U	A_G
Na_2KSb	1.48	0.22	0.52	0.04924
K_2CsSb	1.53	0.23	0.57	0.05354
Rb_2CsSb	1.72	0.26	1.77	0.15057

theoretical studies are also listed in Table II for comparison [57,58]. For Na_2KSb and K_2CsSb, our calculated elastic constants are significantly different from those of Murtaza and coworkers [58], resulting in significant differences in mechanical parameters. However, our results for Na_2KSb are in good agreement with those of Yalameha and coworkers [57]. Furthermore,, these mechanical parameters is proportional to the bonding properties of these compounds, i.e., the stronger the bond, the greater the mechanical parameter [80]. Although we could not find any experimental results for the mechanical properties of both materials, our results are consistent with the above law. Hence, our results are more reliable. However, the difference in elastic properties still needs to be verified by experiments. Furthermore, we found that G_V calculated by Murtaza and coworker has some deviations. We recalculated G_V and G_H and listed it in Table II.

Generally, FH compounds have compelling electronic properties. Hence, we calculated electronic band structure and the corresponding electronic density of states (EDOS) as shown in Fig. 4 for PBEsol results, and Fig. S4 in the Supplemental Material [41] for HSE06 results, respectively. Since the PBEsol functional underestimate band gaps, the HSE06 functional was employed to capture accurate band gaps. These three compounds are all direct band gap semiconductors, and the values of HSE06 band gaps are listed in Table I. From the ELF pictures of these three FH compounds, the electrons of the alkali-metal atoms are more localized, so they contribute less to the valence band maximum (VBM). Due to the strong covalent bond of the Sb anion skeleton, the band structures of these three compounds all show good electron band dispersion, which usually means high conductivity σ and carrier mobility μ. Therefore, we used the electron BTE to calculate the electron transport properties of these three FH compounds, including carrier mobility (μ), electrical conductivity (σ), Seebeck coefficient (S), and electronic thermal conductivity (κ_e). In particular, considering ADP scattering, POP scattering, and IMP scattering, a reasonable electron relaxation time is calculated. The calculated scattering rates for these three FH compounds are shown in Fig. S6 in the Supplemental Material [41]. Because of the large electron band dispersion at conduction band minimum (CBM) for the three FH compounds, we captured anomalously high electron mobility μ_e, especially Na_2KSb, which exceeds 3×10^3 $cm^2\,V^{-1}\,s^{-1}$ at 300 K, as shown in Fig. 5. In addition, the K_2CsSb also has a high μ_e with a value of 487 $cm^2\,V^{-1}\,s^{-1}$ at 300 K.

Following, we turn to investigate TE performance, the calculated σ, S, κ_e, and TE power factor for the three FH compounds are shown in Fig. 6, Fig. S7, and Fig. S8 in the Supplemental Material [41]. Generally, light-mass semiconductors have high σ and μ [35], which are in good agreement with our results. Compared with three p-type FH compounds, the three n-type FH compounds have greater σ due to the greater electronic band dispersion at CBM. In contrast, three p-type counterparts have larger S because of the flatter electron bands at VBM. Analogous to the universal trend observed in most TE materials with semiconducting behavior, the σ ($|S|$) decreases (increases) as temperature increases at the same carrier concentration (n), and increases (decreases) as the n increases at same temperature. Because of the coexistence of large |S| and high σ, a high TE power

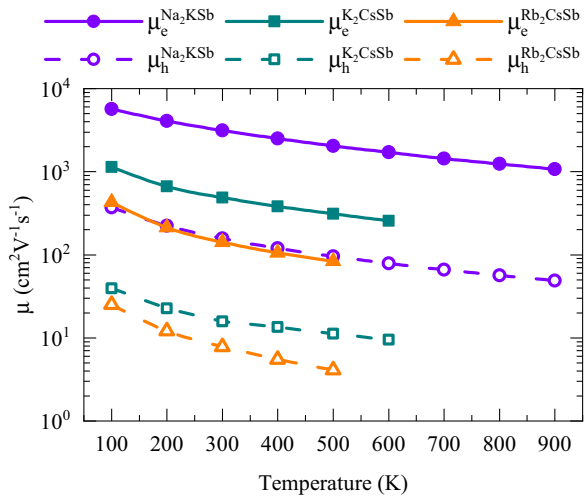

FIG. 5. The calculated carrier mobility (μ_e and μ_h) as a function of temperature for Na_2KSb, K_2CsSb, and Rb_2CsSb.

factor are captured, especially for p-type K_2CsSb, which can reach 2.4 mW m^{-1} K^{-2} at 600 K and optimal carrier concentration n_h. Subsequently, we investigate the electrical thermal conductivity κ_e, because the electron thermal transport is also very eventful to ultimate TE performance. Distinctly, at the same temperature, the κ_e demonstrates the same trend as the σ, that is, as the carrier concentration n increases, the κ_e increases. The above results can be well illustrated by Wiedemann-Franz law (κ_e=LσT), where L is the Lorenz number. The difference is that κ_e is determined by the T and the σ at the same carrier concentration. Because of

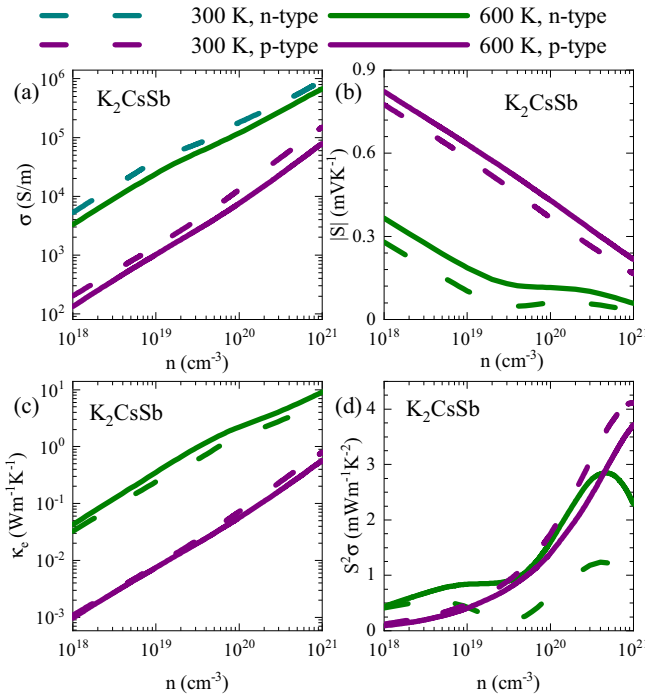

FIG. 6. The calculated (a) electrical conductivity σ, (b) Seebeck coefficient S, (c) electrical thermal conductivity κ_e, and (d) TE power factor σS^2 for K_2CsSb.

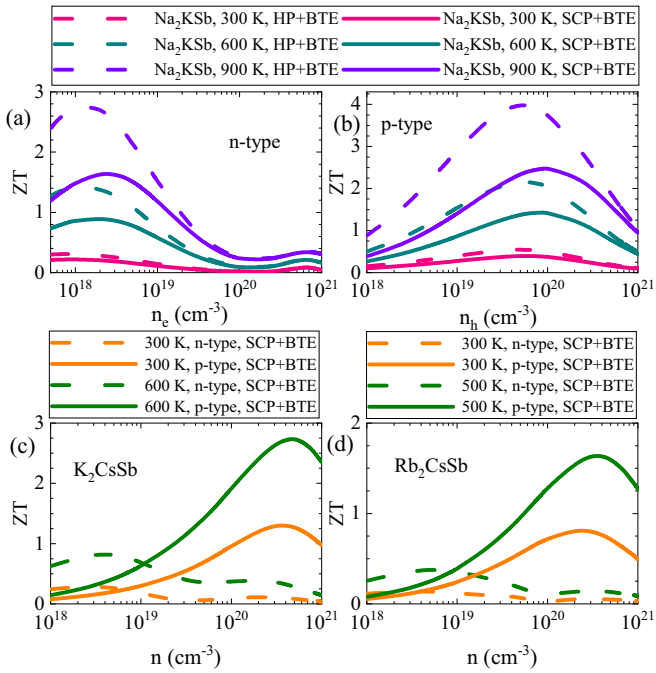

FIG. 7. The calculated TE figure of merit for (a) n-type Na_2KSb, (b) p-type Na_2KSb, (c) K_2CsSb, and (d) Rb_2CsSb.

the contradictory nature of σ, κ_e and S, we need to change the carrier concentration to seek the best thermoelectric performance for these three FH compounds.

Because of the extremely low κ_L combined with high TE power factor, the good TE performance are captured in these three FH compounds, as shown in Fig. 7. Among them, the highest ZT values ~2.74 (1.30) at T = 600 (300) K and $n_h \sim 5 \times 10^{20}$ (4×10^{20}) cm^{-3} are captured in the p-type K_2CsSb. In addition, the p-type Na_2KSb has a high ZT with the value of 2.48 at T = 900 K and $n_h \sim 1 \times 10^{20}$ cm^{-3}. The n-type Na_2KSb also exhibits a good TE performance, and the ZT is 1.65 at T = 900 K and $n_h \sim 2 \times 10^{18}$ cm^{-3}. In addition, we only use the BTE to calculate the electronic transport properties at specific doping concentrations without considering specific p-type and n-type dopants, which also means that further experimental and theoretical explorations are required.

IV. CONCLUSIONS

We have performed the state-of-the-art first-principles calculations to investigate the mechanical, transport and thermoelectric properties in full Heusler compounds Na_2KSb and X_2CsSb (X = K, Rb) by processing the influence of quartic anharmonicity on the phonon energies and capturing a rational electron relaxation time. The calculated results indicate that the strong anharmonicity of alkali-metal atoms is the main reason for their extremely low κ_L. Our study unveils that the alkali-metal atoms play an important role in nonimaginary phonon frequencies for X_2CsSb (X = K, Rb). As the atomic number of alkali-metal increases, the strength of quartic anharmonicity increases. As the atomic number of alkali-metals increases, the strength of the interaction between atoms decreases, and bulk modulus (B), shear modulus (G), and Young's modulus (E) decrease. Taking into account ADP, POP, and IMP scattering, we captured a rational electron relaxation time and transport properties. Because of the large electron dispersion bands at CBM, the anomalously high electronic mobility are captured in p-type for Na_2KSb and K_2CsSb. Finally, an excellent TE performance is predicted in the three p-type FH compounds because of the combination of extremely low lattice thermal conductivity and good TE power factor. In addition, the n-type Na_2KSb has good TE properties. The calculated results support them as potential candidates for thermal management and thermoelectric applications.

ACKNOWLEDGMENTS

This research was supported by the National Natural Science Foundation of China under Grants No. 11974302 and No. 12174327.

[1] J. G. Zivin and M. Neidell, Science **359**, 39 (2018).
[2] G. A. Lincoln, Science **180**, 155 (1973).
[3] F. Li, J.-F. Li, L.-D. Zhao, K. Xiang, Y. Liu, B.-P. Zhang, Y.-H. Lin, C.-W. Nan, and H.-M. Zhu, Energy Environ. Sci. **5**, 7188 (2012).
[4] J.-S. Rhyee, K. H. Lee, S. M. Lee, E. Cho, S. I. Kim, E. Lee, Y. S. Kwon, J. H. Shim, and G. Kotliar, Nature (London) **459**, 965 (2009).
[5] J. Sootsman, D. Chung, and M. Kanatzidis, Angew. Chem., Int. Ed. **48**, 8616 (2009).
[6] L.-D. Zhao, J. He, D. Berardan, Y. Lin, J.-F. Li, C.-W. Nan, and N. Dragoe, Energy Environ. Sci. **7**, 2900 (2014).
[7] Y. Zhang, J.-H. Bahk, J. Lee, C. S. Birkel, M. L. Snedaker, D. Liu, H. Zeng, M. Moskovits, A. Shakouri, and G. D. Stucky, Adv. Mater. **26**, 2755 (2014).
[8] J.-H. Bahk, Z. Bian, and A. Shakouri, Phys. Rev. B **89**, 075204 (2014).
[9] C. Kumarasinghe and N. Neophytou, Phys. Rev. B **99**, 195202 (2019).
[10] Y. Xiao, D. Wang, Y. Zhang, C. Chen, S. Zhang, K. Wang, G. Wang, S. J. Pennycook, G. J. Snyder, H. Wu, and L.-D. Zhao, J. Am. Chem. Soc. **142**, 4051 (2020).
[11] J. L. Niedziela, D. Bansal, J. Ding, T. Lanigan-Atkins, C. Li, A. F. May, H. Wang, J. Y. Y. Lin, D. L. Abernathy, G. Ehlers, A. Huq, D. Parshall, J. W. Lynn, and O. Delaire, Phys. Rev. Materials **4**, 105402 (2020).
[12] O. Delaire, J. Ma, K. Marty, A. F. May, M. A. McGuire, M.-H. Du, D. J. Singh, A. Podlesnyak, G. Ehlers, M. Lumsden *et al.*, Nat. Mater. **10**, 614 (2011).
[13] C. W. Li, J. Hong, A. F. May, D. Bansal, S. Chi, T. Hong, G. Ehlers, and O. Delaire, Nat. Phys. **11**, 1063 (2015).
[14] M. S. Toprak, C. Stiewe, D. Platzek, S. Williams, L. Bertini, E. Müller, C. Gatti, Y. Zhang, M. Rowe, and M. Muhammed, Adv. Funct. Mater. **14**, 1189 (2004).

[15] T. Jia, J. Carrete, Z. Feng, S. Guo, Y. Zhang, and G. K. H. Madsen, Phys. Rev. B **102**, 125204 (2020).

[16] S. Mukhopadhyay, D. Bansal, O. Delaire, D. Perrodin, E. Bourret-Courchesne, D. J. Singh, and L. Lindsay, Phys. Rev. B **96**, 100301(R) (2017).

[17] P.-F. Lory, V. M. Giordano, P. Gille, H. Euchner, M. Mihalkovič, E. Pellegrini, M. Gonzalez, L.-P. Regnault, P. Bastie, H. Schober, S. Pailhes, M. R. Johnson, Y. Grin, and M. de Boissieu, Phys. Rev. B **102**, 024303 (2020).

[18] L. Bjerg, B. B. Iversen, and G. K. H. Madsen, Phys. Rev. B **89**, 024304 (2014).

[19] F. Garmroudi, A. Riss, M. Parzer, N. Reumann, H. Müller, E. Bauer, S. Khmelevskyi, R. Podloucky, T. Mori, K. Tobita, Y. Katsura, and K. Kimura, Phys. Rev. B **103**, 085202 (2021).

[20] C. S. Lue, C. F. Chen, J. Y. Lin, Y. T. Yu, and Y. K. Kuo, Phys. Rev. B **75**, 064204 (2007).

[21] F. Gucci, T. G. Saunders, B. Srinivasan, F. Cheviré, D. A. Ferluccio, J.-W. G. Bos, and M. J. Reece, J. Alloys Compd. **837**, 155058 (2020).

[22] P. D. Patel, S. B. Pillai, S. M. Shinde, S. D. Gupta, and P. K. Jha, Phys. B: Condens. Matter **550**, 376 (2018).

[23] J. He, M. Amsler, Y. Xia, S. S. Naghavi, V. I. Hegde, S. Hao, S. Goedecker, V. Ozoliņš, and C. Wolverton, Phys. Rev. Lett. **117**, 046602 (2016).

[24] J. Park, Y. Xia, A. M. Ganose, A. Jain, and V. Ozoliņš, Phys. Rev. Appl. **14**, 024064 (2020).

[25] J. Park, Y. Xia, and V. Ozoliņš, Phys. Rev. Applied **11**, 014058 (2019).

[26] W. Wang, Z. Dai, X. Wang, Q. Zhong, Y. Zhao, and S. Meng, Int. J. Energy Res. **45**, 20949 (2021).

[27] W. H. McCarroll and R. E. Simon, Rev. Sci. Instrum. **35**, 508 (1964).

[28] G. Xing, J. Sun, Y. Li, X. Fan, W. Zheng, and D. J. Singh, Phys. Rev. Materials **1**, 065405 (2017).

[29] O. Madelung, Ix-Vy compounds, in *Semiconductors: Data Handbook* (Springer, Berlin, 2004) pp. 437–445.

[30] F. Zhang, X.-P. Li, and X.-S. Li, Chinese Phys. Lett. **36**, 022901 (2019).

[31] Z. Ding, M. Gaowei, J. Sinsheimer, J. Xie, S. Schubert, H. Padmore, E. Muller, and J. Smedley, J. Appl. Phys. **121**, 055305 (2017).

[32] C. W. Morrison, J. Appl. Phys. **37**, 713 (1966).

[33] M. K. Jana, K. Pal, U. V. Waghmare, and K. Biswas, Angew. Chem., Int. Ed. **55**, 7792 (2016).

[34] Z. Feng, Y. Fu, Y. Zhang, and D. J. Singh, Phys. Rev. B **101**, 064301 (2020).

[35] Z. Feng, Y. Fu, Y. Yan, Y. Zhang, and D. J. Singh, Phys. Rev. B **103**, 224101 (2021).

[36] E. S. Toberer, A. Zevalkink, N. Crisosto, and G. J. Snyder, Adv. Funct. Mater. **20**, 4375 (2010).

[37] G. Kresse and D. Joubert, Phys. Rev. B **59**, 1758 (1999).

[38] G. I. Csonka, J. P. Perdew, A. Ruzsinszky, P. H. T. Philipsen, S. Lebègue, J. Paier, O. A. Vydrov, and J. G. Ángyán, Phys. Rev. B **79**, 155107 (2009).

[39] G. Kresse and J. Furthmüller, Phys. Rev. B **54**, 11169 (1996).

[40] G. Kresse and J. Furthmüller, Comput. Mater. Sci. **6**, 15 (1996).

[41] See Supplemental Material at http://link.aps.org/supplemental/10.1103/PhysRevB.105.184304 for the calculating method of different scattering rate and transport coefficients, as well as the AIMD simulations, thermal transport parameters, the cumulative thermal conductivities, the electron localization functions, energy band structures, and the electron scattering rate for Na_2KSb and X_2CsSb (X=K,Rb).

[42] S. Baroni, S. de Gironcoli, A. Dal Corso, and P. Giannozzi, Rev. Mod. Phys. **73**, 515 (2001).

[43] W. McCarroll, J. Phys. Chem. Solids **16**, 30 (1960).

[44] A. R. H. F. Ettema and R. A. de Groot, Phys. Rev. B **66**, 115102 (2002).

[45] W. McCarroll, J. Phys. Chem. Solids **26**, 191 (1965).

[46] K. Esfarjani and H. T. Stokes, Phys. Rev. B **77**, 144112 (2008).

[47] F. Zhou, B. Sadigh, D. Åberg, Y. Xia, and V. Ozoliņš, Phys. Rev. B **100**, 184309 (2019).

[48] T. Tadano and S. Tsuneyuki, Phys. Rev. B **92**, 054301 (2015).

[49] T. Tadano, Y. Gohda, and S. Tsuneyuki, J. Phys.: Condens. Matter **26**, 225402 (2014).

[50] A. M. Ganose, J. Park, A. Faghaninia, R. Woods-Robinson, K. A. Persson, and A. Jain, Nat. Commun. **12**, 2222 (2021).

[51] G. K. Madsen, J. Carrete, and M. J. Verstraete, Comput. Phys. Commun. **231**, 140 (2018).

[52] T. Tadano and S. Tsuneyuki, Phys. Rev. Lett. **120**, 105901 (2018).

[53] M. Christensen, A. B. Abrahamsen, N. B. Christensen, F. Juranyi, N. H. Andersen, K. Lefmann, J. Andreasson, C. R. Bahl, and B. B. Iversen, Nat. Mater. **7**, 811 (2008).

[54] L. Novotny, Am. J. Phys. **78**, 1199 (2010).

[55] F. Mouhat and F.-X. Coudert, Phys. Rev. B **90**, 224104 (2014).

[56] Z.-j. Wu, E.-j. Zhao, H.-p. Xiang, X.-f. Hao, X.-j. Liu, and J. Meng, Phys. Rev. B **76**, 054115 (2007).

[57] S. Yalameha, Z. Nourbakhsh, and A. Vaez, J. Magn. Magn. Mater. **468**, 279 (2018).

[58] G. Murtaza, M. Ullah, N. Ullah, M. Rani, M. Muzammil, R. Khenata, S. M. Ramay, and U. Khan, Bull. Mater. Sci. **39**, 1581 (2016).

[59] K. Momma and F. Izumi, J. Appl. Crystallogr. **41**, 653 (2008).

[60] Y. Xia, K. Pal, J. He, V. Ozoliņš, and C. Wolverton, Phys. Rev. Lett. **124**, 065901 (2020).

[61] Y. Zhao, S. Zeng, G. Li, C. Lian, Z. Dai, S. Meng, and J. Ni, Phys. Rev. B **104**, 224304 (2021).

[62] Y. Hu, Y. Jin, G. Zhang, and Y. Yan, RSC Adv. **10**, 28501 (2020).

[63] Y. Shimanuki, K. Kudo, T. Ishibe, A. Masago, S. Yamada, Y. Nakamura, and K. Hamaya, J. Appl. Phys. **127**, 055106 (2020).

[64] Y. Nishino, S. Deguchi, and U. Mizutani, Phys. Rev. B **74**, 115115 (2006).

[65] W. Li, S. Lin, M. Weiss, Z. Chen, J. Li, Y. Xu, W. G. Zeier, and Y. Pei, Adv. Energy Mater. **8**, 1800030 (2018).

[66] X. Zhang, Z. Chen, S. Lin, B. Zhou, B. Gao, and Y. Pei, ACS Energy Lett. **2**, 2470 (2017).

[67] J. Ranninger, Phys. Rev. **140**, A2031 (1965).

[68] A. Jain and A. J. H. McGaughey, J. Appl. Phys. **116**, 073503 (2014).

[69] R. Osborn, E. A. Goremychkin, A. I. Kolesnikov, and D. G. Hinks, Phys. Rev. Lett. **87**, 017005 (2001).

[70] H. Shang, J. Zhao, and J. Yang, J. Phys. Chem. C **125**, 6479 (2021).

[71] S. Aria Hosseini, S. Khanniche, P. Alex Greaney, and G. Romano, Int. J. Heat Mass Transf. **183**, 122040 (2022).

[72] S. A. Hosseini, G. Romano, and P. A. Greaney, ACS Appl. Energy Mater. **4**, 1915 (2021).
[73] S. A. Hosseini, G. Romano, and P. A. Greaney, Nanomaterials **11**, 2591 (2021).
[74] D. H. Chung and W. R. Buessem, J. Appl. Phys. **38**, 2535 (1967).
[75] A. Reuss, Z. Angew. Math. Mech. **9**, 49 (1929).
[76] R. Hill, Proc. Phys. Soc. Sect. A **65**, 349 (1952).
[77] S. Pugh, Philos. Mag. J. Sci. **45**, 823 (1954).
[78] J. Haines, J. Léger, and G. Bocquillon, Annu. Rev. Mater. Res. **31**, 1 (2001).
[79] P. Ravindran, L. Fast, P. A. Korzhavyi, B. Johansson, J. Wills, and O. Eriksson, J. Appl. Phys. **84**, 4891 (1998).
[80] K. Panda and K. R. Chandran, Acta Mater. **54**, 1641 (2006).

Correction: Labels for the first and second corresponding authors were missing and have been inserted.